AFRL-RI-RS-TR-2020-097

ENABLING FREQUENCY-AGILE ULTRA-BROADBAND AIRBORNE NETWORKS IN THE THZ BAND

RESEARCH FOUNDATION FOR THE STATE UNIVERSITY OF NEW YORK

JUNE 2020

FINAL TECHNICAL REPORT

APPROVED FOR PUBLIC RELEASE; DISTRIBUTION UNLIMITED

STINFO COPY

AIR FORCE RESEARCH LABORATORY
INFORMATION DIRECTORATE

■ **AIR FORCE MATERIEL COMMAND** ■ **UNITED STATES AIR FORCE** ■ **ROME, NY 13441**

The system blocks mostly affecting the capabilities are:

- **NI PXIe-3610:** The PXIe-3610 is a 14 bit DAC with a sampling rate of 3.072 GSa/s and can support 2 GHz bandwidth. At the transmitter, this module along with the PXIe-3620 acts as an arbitrary waveform generator.
- **NI PXIe-3630:** The PXIe-3630 is a 12 bit ADC with a sampling rate of 3.072 GSa/s and can also support 2GHz bandwidth. At the receiver, this module along with the PXIe-3620 acts as a digitizer.
- **NI PXIe-3620:** This module provides an IF interface operating in the range of 10.5 GHz to 12 GHz frequencies. The IF OUT port supports a linear power in the range -40 dBm to 7 dBm and the IF IN port supports -25 dBm to +20 dBm linear power. It is capable of working in a full-duplex mode with 2GHz of instantaneous bandwidth.
- **NI PXIe-7902:** The NI chassis has two NI PXIe-7902 modules, each housing Xilinx Virtex 7 485T FPGA, one acting as modulator and one as demodulator. The Modulator FPGA modulates the signal and sends it to the PXIe-3610 (DAC) for transmission, whereas the Demodulator FPGA demodulates the signal received from the PXIe-3630 (ADC). Currently, the system supports conventional phase and amplitude modulations, including BPSK, QPSK, 8PSK, 16QAM and 64QAM. Later in the project, these modules will be reprogrammed according to our newly designed modulations.
- **NI PXIe-7976R:** The NI chassis incorporates several NI PXIe-7976R modules, in charge of error control and any additional required digital signal processing. In terms of error control, Turbo Codes and Cyclic Redundancy Check are currently implemented. Additional signal processing might be related to, among others, the implementation of multi-carrier modulations including OFDM, which is part of this project too.

The control of the system and programming of reconfigurable modules (NI PXIe-7902 and -7976R) is performed through NI LabView.

3.1.2 Up- and Down-converting System at 1 THz

We currently have access to an up-converter and a down-converter at 1 THz, which are utilized at the transmitter and the receiver respectively. On the transmitter side, an analog signal generator (PSG, Keysight E8257D) with very low root mean square (RMS) jitter (21 fs) is utilized to synthesize the Local Oscillator (LO) at a frequency between 41.67 GHz and 43.75 GHz. A Schottky-diode-based chain of frequency multipliers, custom designed by Virginia Diode Inc. (VDI), is utilized to upconvert the LO to the target radio frequency (RF) between 1 THz and 1.05 THz. A mixer based on the same technology is utilized to mix an Intermediate Frequency (IF) signal. The maximum input power at IF in the mixer is 0 dBm and the maximum output power is -15 dBm or 30 μW. On the receiver side, a second PSG and a frequency multiplier chain with mixer based on the same technology is utilized to generate the LO frequency and RF carrier, respectively, needed to down-convert the received RF frequency to IF band. Furthermore, for transmitting and receiving the RF signal, two directional diagonal horn antennas (by VDI) are utilized. Both antennas exhibits 26 dBi gain and 10 degree angle half-power bandwidth at the 1 THz design frequency. Coaxial

(2.4 mm male to male) and RoHS (restriction of hazardous substances) compliant cables are utilized to interconnect the different testbed elements.

3.1.3 Interconnection of the two Systems

The following hardware and software modifications have been implemented (Figure 1). On the transmitter side, the NI LabView software project has been modified for the NI baseband to output the IF signals through the NI PXIe-3610 and the output of the NI PXIe-3620 has been interfaced with the VDI mixer. On the receiver side, the VDI mixer output has been connected to the NI PXIe-3630 and the software has been modified accordingly to process the received signals at IF.

3.2 Results and Discussion

Currently, 2-GHz-wide signals following a TDMA scheme are transmitted and received. The system uses a 10 ms frame with 100 slots. Each slot is 100 μs long and contains 150 blocks. Different blocks can serve different purposes, including synchronization, channel estimation and uplink and downlink data (the current system is half-duplex only). At the time this report is written, successful data transmission has been accomplished utilizing single-carrier modulations (see Figure 2), but only for the data slots transmitted immediately after a synchronization slot (Figure 3). We are currently exploring the trade-offs between synchronization, channel estimation and data-slots.

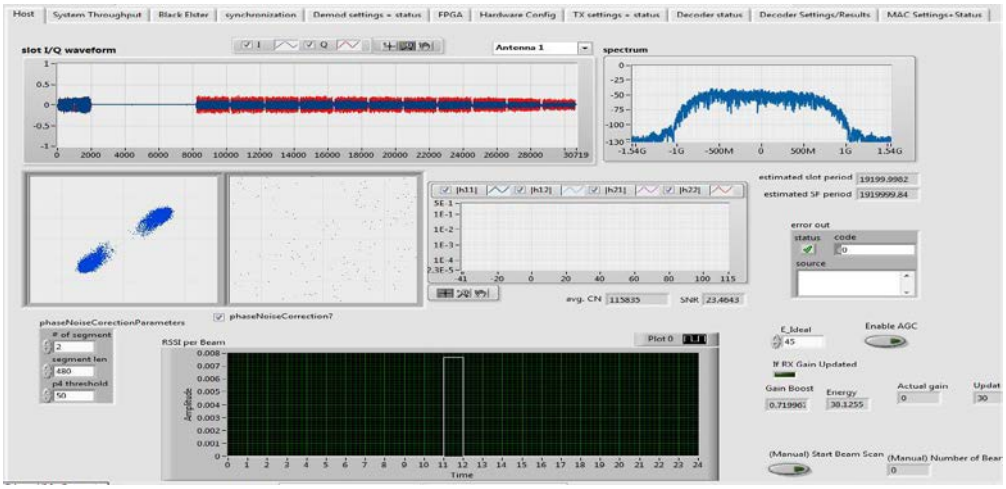

Fig. 2: Successful data blocks transmission following a synchronization block.

Fig. 3: Periodic successful and unsuccessful blocks transmission within one frame.

4 HIERARCHICAL BANDWIDTH MODULATION DESIGN

4.1 Methods, Assumptions and Procedures

The peculiarities of the THz-band channel [19] motivate the development of new modulation schemes. While traditional modulations (e.g., m-PSK, m-QAM) can be utilized, these cannot make the most of the unique behavior of the available bandwidth at THz frequencies. More specifically, in airborne networks, the available bandwidth changes with both the distance between the transmitter and the receiver as well as their absolute and relative altitude. This phenomenon leads to different types of communication links, including, *horizontal links* between planes at the same altitude and *vertical links* between planes at different altitudes. Therefore, in order to maximize the utilization of the air-to-air channel, distance- and altitude-adaptive dynamic-bandwidth modulations are needed. During this reporting period, we have established the fundamental theoretical basis of hierarchical bandwidth modulations. Partially related to the concept of hierarchical or concatenated modulations [32], the fundamental idea in this case is to embed multiple binary information streams on the same carrier signal while adjusting the symbol time according to the available bandwidth. Hierarchical modulations are traditionally used in video transmission over the air, as a way to guarantee that receivers with different capabilities and channel conditions can display the content to the best of their resources. In our case, not only the modulation order can be adapted to the received signal strength, but, more importantly, the symbol transmission rate is set in light of the available bandwidth.

Next, we describe the modulator and demodulator designs and provide preliminary performance results.

4.1.1 Modulator and Demodulator Block Diagrams

The conceptual block diagram of the hierarchical bandwidth modulator is shown in Fig. 4. The figure depicts an M-level modulator in which a QPSK modulation is chosen to be the base layer modulation and $r_1 > r_2 > r_3 > \ldots > r_M$, where r_i is the distance between the transmitter and the ith receiver.

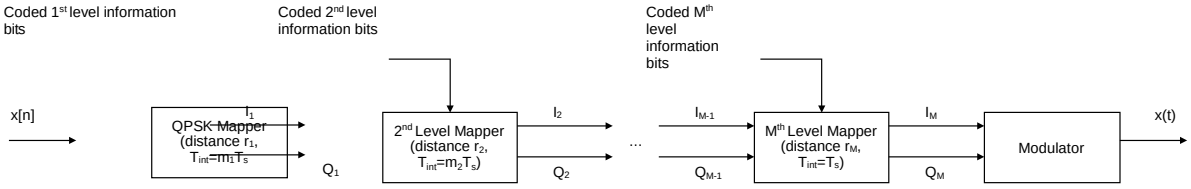

Fig. 4: Block diagram for the hierarchical bandwidth modulator.

The outputs of the first block are the I and Q components of the base modulation, which are held constant for a total symbol time of m_1T_s, where m_1 is an integer and T_s is the inverse of the bandwidth available at the closest receiver. The second mapping block further modulates the I and Q components according to the second level of information. In other words, each QPSK symbol is further mapped to a local QPSK modulation. In this case, the information bits are held for a total symbol time of m_2T_s. Note that, m_1 must be an integer multiple of m_2. This is applied successively until the highest level modulation, M, whose symbols are held only for Ts. For a fixed transmission power, the fact that higher level modulations are held for shorter times results into a lower transmission energy per bit Eb. However, over the shorter distances at which these symbols are expected to be received, the channel path-loss is lower, which results in still high E_b/N_0 values at the receiver.

On the receiver side, as shown in Fig. 5, the first step is to estimate the bandwidth $\frac{1}{T_s}$ of the received signal, which in the simplest case could be done by means of a training pulse sequence. Based on the estimated factor $m = T_s'/T_s$, the received signal is then demodulated as a $4^{(M-m+1)}$QAM at a $\frac{1}{mT_s}$ rate. A traditional M-level hierarchical modulator maps all the layers at the same rate that is suitable for the farthest receiver. In the considered scenario, this rate would be $\frac{1}{MT_s}$, where $\frac{1}{T_s}$ is the rate available for closest receiver. On the receiver side, the demodulator would estimate the bandwidth $\frac{1}{T_s'}$ to get an estimate of the distance ($m = T'/T_s$) and in turn to decide on the demodulator ($4^{(M-m+1)}$QAM). However, the symbol duration would still be MT_s for all of the M receivers.

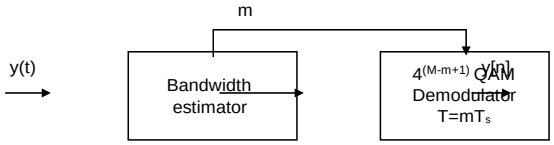

Fig. 5: Block diagram for the hierarchical bandwidth demodulator.

4.2 Results and Discussion

We next numerically illustrate and analyze the performance of hierarchical bandwidth modulations. The carrier frequency is chosen to be 1.025 THz. Considering that the channel bandwidth is chopped almost to half from 1 m to 30 m distance, we place two receivers at distance 1 m and 30 m. The bandwidth available at the closer and farther receivers is 92 GHz and 45 GHz respectively. We set the transmission power to 1 mW, in light of the existing compact THz sources at room temperature. We consider the transmitter and the receiver to be equipped with directional antennas with 30 dB, which enable meeting the SNR requirement at the furthest receiver. The THz channel is numerically implemented by following our model in [19].

In Fig. 6, we illustrate the time and frequency domain representation of the transmitted signal, the received signal at 1 m and the received signal at 30 m, respectively. From this figure, it is clear that not only the received signal power is much lower, but its bandwidth has been drastically reduced. This is due to the high frequency components being chopped by the molecular absorption of THz channel. This phenomenon is clearer from the frequency domain plot of the signals in fig. 6d, 6e, and 6f. As a result, the user at 30 m distance can not receive the enhancement layer information, rather bound to demodulate the base layer information at rate $\frac{1}{2T_s}$.

The symbol error rate (SER) for the closer and the farther users are shown in Figure 7 as function of the SNR for farther receiver. It is relevant to note that, when the SNR requirement for the farther user is met, it is also being met for the closer user. As can be seen from this figure, the closer receiver has no error until the SNR for farther receiver goes as bad as -6 dB which would never be the target. To see this better, the received constellation diagrams at the closer and farther receiver is shown in Fig. 8a and Fig. 8b respectively for an SNR of 18 dB at the farther node.

For the full detailed analysis, we point the reader to our work in [33]. Our next steps involve the implementation of this modulation and testing in the experimental platform described in Sec. 3.

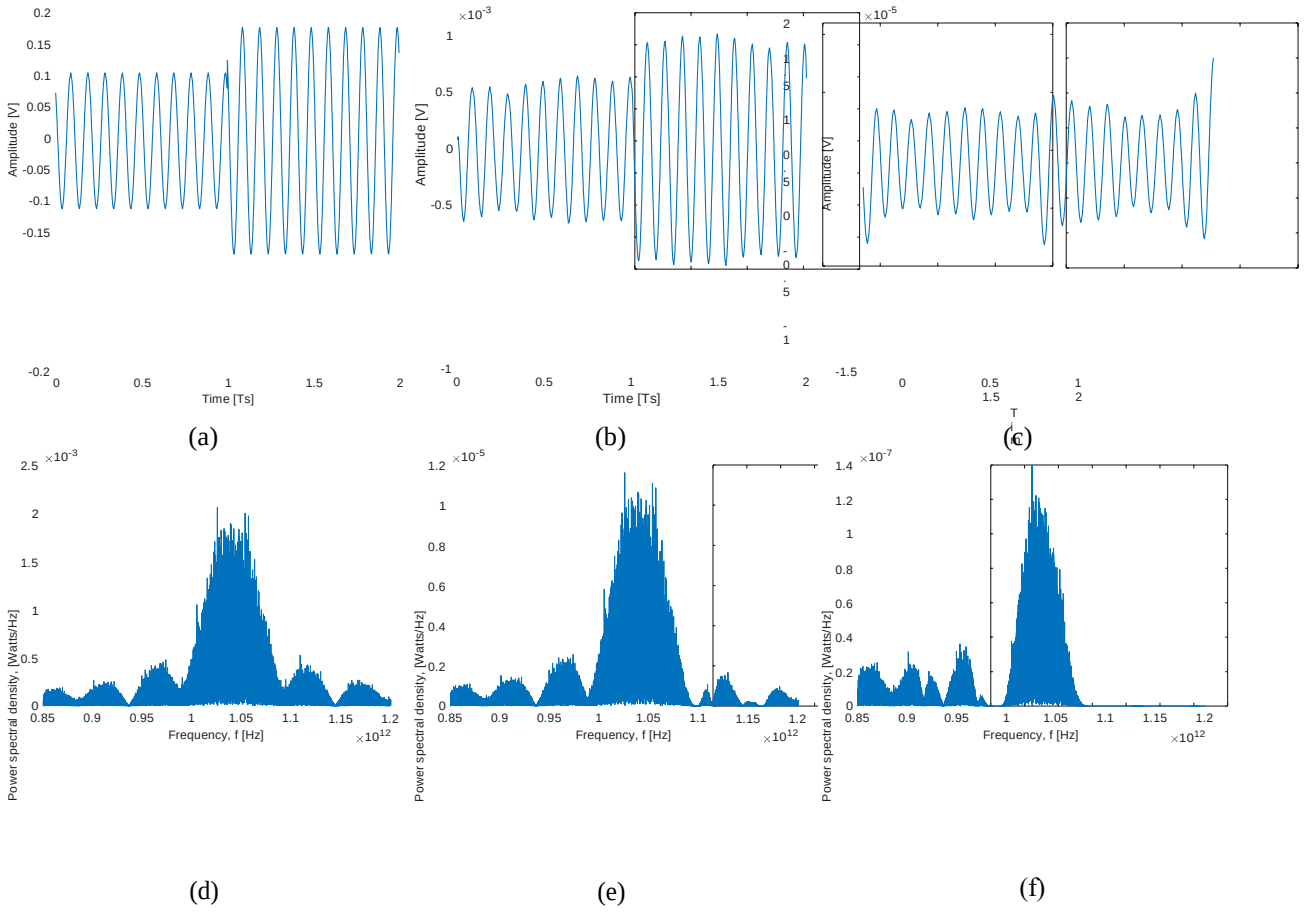

Fig. 6: Time and frequency domain plot of the transmitted signal, received signal at 1 m and received signal at 30 m.

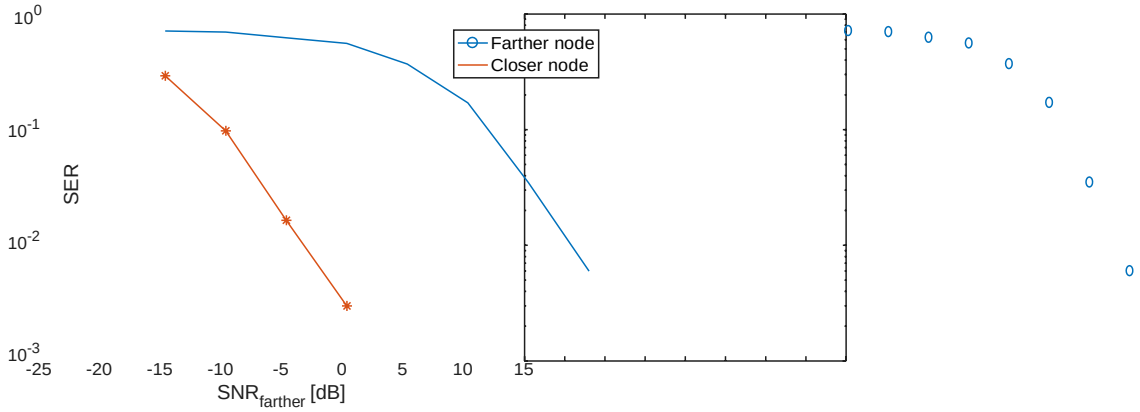

Fig. 7: SER of both closer and farther receiver as a function of SNR of farther receiver.

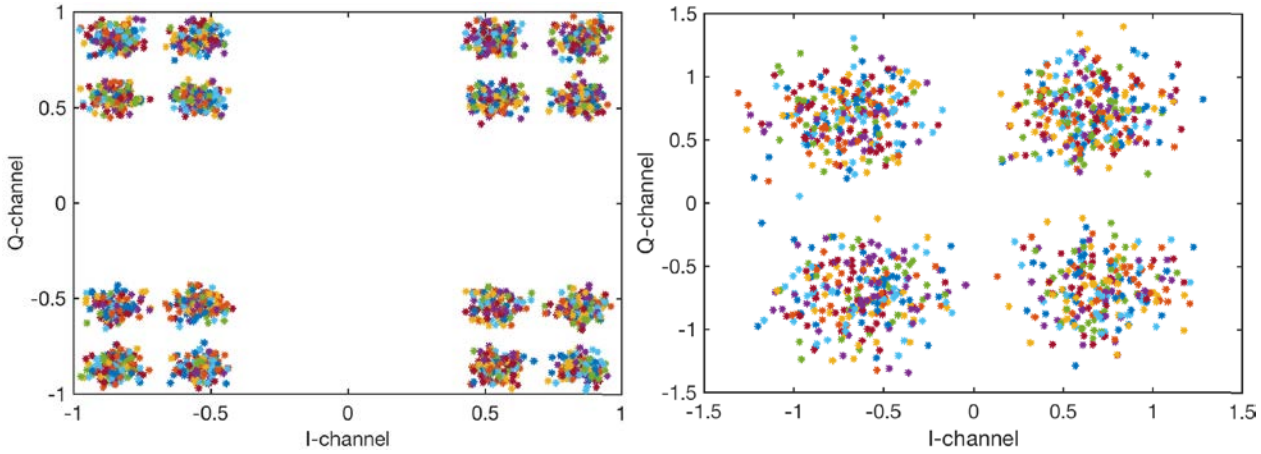

(a) Closer receiver.

(b) Farther receiver.

Fig. 8: Received constellations.

5 CONCLUSIONS

THz communications will contribute to realize the vision of the Air Force Future Operating Concept in different ways [34]. On the one hand, the addition of a new spectral band can relieve the overcrowded spectrum at lower frequencies and, thus, increase the performance of legacy systems. On the other hand, THz communication enables new high-bandwidth applications that are not feasible with current narrow-band wireless technologies, such as in-air big-data sharing among networks of unmanned aircrafts for real-time monitoring, decision and actuation. Ultimately, this will help to diversify the portfolio of capabilities needed to achieve operational agility. Beyond the US Air Force, and as highlighted in the recent report by the National Institute of Standards and Technology (NIST) on Future Generation Wireless Research and Development Gap ([35], Section 2.2.2, Higher Frequencies), *future generation networks will need to leverage higher frequencies (above 6 GHz and up to THz) in conjunction with existing technologies (below 6 GHz) in order to meet the performance expectations of seamless user connectivity, improved speed, and ultra-reliability.*

Within the first five months of the project, the focus has been on developing the experimental platform to be utilized for the testing and refinement of the new networking protocols for airborne THz networks as well as on the theoretical and numerical analysis of new modulations that can make the most of the THz channel and its distance-dependent bandwidth. Moving forward, contributions will be made along the theoretical design and experimental implementation and testing of tailored networking protocols for mobile airborne THz communication networks.

6. REFERENCES

[1] R. Piesiewicz, T. Kleine-Ostmann, N. Krumbholz, D. Mittleman, M. Koch, J. Schoebei, and T. Kurner, "Short-range ultra-broadband terahertz communications: Concepts and perspectives," *IEEE Antennas and Propagation Magazine*, vol. 49, no. 6, pp. 24–39, 2007.

[2] J. Federici and L. Moeller, "Review of terahertz and subterahertz wireless communications," *Journal of Applied Physics*, vol. 107, no. 11, p. 111101, 2010.

[3] H.-J. Song and T. Nagatsuma, "Present and future of terahertz communications," *IEEE Transactions on Terahertz Science and Technology*, vol. 1, no. 1, pp. 256–263, 2011.

[4] I. F. Akyildiz, J. M. Jornet, and C. Han, "Terahertz band: Next frontier for wireless communi- cations," *Physical Communication (Elsevier) Journal*, vol. 12, pp. 16–32, Sep. 2014.

[5] T. S. Rappaport, Y. Xing, O. Kanhere, S. Ju, A. Madanayake, S. Mandal, A. Alkhateeb, and G. C. Trichopoulos, "Wireless communications and applications above 100 ghz: Opportunities and challenges for 6g and beyond," *IEEE Access*, vol. 7, pp. 78 729–78 757, 2019.

[6] A. Nikpaik, A. H. M. Shirazi, A. Nabavi, S. Mirabbasi, and S. Shekhar, "A 219-to-231 ghz frequency-multiplier-based vco with˜ 3% peak dc-to-rf efficiency in 65-nm cmos," *IEEE Journal of Solid-State Circuits*, vol. 53, no. 2, pp. 389–403, 2018.

[7] H. Aghasi, A. Cathelin, and E. Afshari, "A 0.92-thz sige power radiator based on a nonlinear theory for harmonic generation," *IEEE Journal of Solid-State Circuits*, vol. 52, no. 2, pp. 406–422, 2017.

[8] W. R. Deal, K. Leong, A. Zamora, B. Gorospe, K. Nguyen, and X. B. Mei, "A 660 ghz up-converter for thz communications," in *Compound Semiconductor Integrated Circuit Symposium (CSICS), 2017 IEEE*. IEEE, 2017, pp. 1–4.

[9] A. Leuther, A. Tessmann, P. Doria, M. Ohlrogge, M. Seelmann-Eggebert, H. Maßler, M. Schlechtweg, and O. Ambacher, "20 nm metamorphic hemt technology for terahertz monolithic integrated circuits," in *9th IEEE European Microwave Integrated Circuit Confer- ence (EuMIC)*. IEEE, 2014, pp. 84–87.

[10] M. Urteaga, Z. Griffith, M. Seo, J. Hacker, and M. J. Rodwell, "Inp hbt technologies for thz integrated circuits," *Proceedings of the IEEE*, vol. 105, no. 6, pp. 1051–1067, 2017.

[11] I. Mehdi, J. V. Siles, C. Lee, and E. Schlecht, "Thz diode technology: status, prospects, and applications," *Proceedings of the IEEE*, vol. 105, no. 6, pp. 990–1007, 2017.

[12] H.-J. Song, K. Ajito, Y. Muramoto, A. Wakatsuki, T. Nagatsuma, and N. Kukutsu, "Uni-travelling-carrier photodiode module generating 300 ghz power greater than 1 mw," *IEEE Microwave and Wireless Components Letters*, vol. 22, no. 7, pp. 363–365, 2012.

[13] S.-W. Huang, J. Yang, S.-H. Yang, M. Yu, D.-L. Kwong, T. Zelevinsky, M. Jarrahi, and C. W. Wong, "Globally stable microresonator turing pattern formation for coherent high-power thz radiation on-chip," *Physical Review X*, vol. 7, no. 4, p. 041002, 2017.

[14] T. Nagatsuma, G. Ducournau, and C. C. Renaud, "Advances in terahertz communications accelerated by photonics," *Nature Photonics*, vol. 10, no. 6, p. 371, 2016.

[15] Q. Lu, D. Wu, S. Sengupta, S. Slivken, and M. Razeghi, "Room temperature continuous wave, monolithic tunable THz sources based on highly efficient mid-infrared quantum cascade lasers," *Scientific reports*, vol. 6, 2016.

[16] A. C. Ferrari, F. Bonaccorso, V. Fal'Ko, K. S. Novoselov, S. Roche, P. Bøggild, S. Borini, F. H. Koppens, V. Palermo, N. Pugno *et al.*, "Science and technology roadmap for graphene, related two-dimensional crystals, and hybrid systems," *Nanoscale*, vol. 7, no. 11, pp. 4598–4810, 2015.

[17] J. M. Jornet and I. F. Akyildiz, "Graphene-based plasmonic nano-transceiver for terahertz band communication," in *Proc. of European Conference on Antennas and Propagation (EuCAP)*, 2014, U.S. Patent No. 9,397,758, July 19, 2016 (Priority Date: Dec. 6, 2013).

[18] J. M. Jornet and I. F. Akyildiz, "Graphene-based plasmonic nano-antenna for terahertz band communication in nanonetworks," *IEEE JSAC, Special Issue on Emerging Technologies for Communications*, vol. 12, no. 12, pp. 685–694, Dec. 2013, U.S. Patent No. 9,643,841, May 9, 2017 (Priority Date: Dec. 6, 2013).

[19] J. M. Jornet and I. F. Akyildiz, "Channel modeling and capacity analysis of electromagnetic wireless nanonetworks in the terahertz band," *IEEE Transactions on Wireless Communications*, vol. 10, no. 10, pp. 3211–3221, Oct. 2011.

[20] C. Han, A. O. Bicen, and I. Akyildiz, "Multi-ray channel modeling and wideband characteri- zation for wireless communications in the terahertz band," *IEEE Transactions on Wireless Communications*, vol. 14, no. 5, pp. 2402–2412, May 2015.

[21] Z. Hossain, C. Mollica, and J. M. Jornet, "Stochastic multipath channel modeling and power delay profile analysis for terahertz-band communication (best paper award)," in *Proc. of the 4th ACM International Conference on Nanoscale Computing and Communications (NanoCom)*, Sep. 2017.

[22] J. M. Jornet and I. F. Akyildiz, "Femtosecond-long pulse-based modulation for terahertz band communication in nanonetworks," *IEEE Transactions on Communications*, vol. 62, no. 5, pp. 1742–1754, May 2014.

[23] C. Han and I. F. Akyildiz, "Distance-aware bandwidth-adaptive resource allocation for wireless systems in the terahertz band," *IEEE Transactions on Terahertz Science and Technology*, vol. 6, no. 4, 2016.

[24] N. Akkari, J. Jornet, P. Wang, E. Fadel, L. Elrefaei, M. Malik, S. Almasri, and I. Akyildiz, "Joint physical and link layer error control analysis for nanonetworks in the terahertz band," *Wireless Networks*, pp. 1–13, 2015.

[25] A. Gupta, M. Medley, and J. M. Jornet, "Joint synchronization and symbol detection design for pulse-based communications in the THz band," in *Proc. of IEEE GLOBECOM*, 2015.

[26] C. Han, I. F. Akyildiz, and W. H. Gerstacker, "Timing acquisition and error analysis for

pulse-based Terahertz band wireless systems," *IEEE Transactions on Vehicular Technology*, vol. 66, no. 11, 2017.

[27] I. F. Akyildiz and J. M. Jornet, "Realizing ultra-massive (MIMO 1024 1024 communication in the (0.06–10) terahertz band," *Nano Communication Networks*, vol. 8, pp. 46–54, 2016, U.S. Patent No. 9,825,712, November 21, 2017 (Priority Date: Dec. 6, 2013).

[28] V. Petrov, M. Komarov, D. Moltchanov, J. M. Jornet, and Y. Koucheryavy, "Interference and SINR in millimeter wave and terahertz communication systems with blocking and directional antennas," *IEEE Transactions on Wireless Communications*, vol. 16, no. 3, pp. 1791–1808, 2017.

[29] Z. Hossain, C. N. Mollica, J. F. Federici, and J. M. Jornet, "Stochastic interference modeling and experimental validation for pulse-based terahertz communication," *IEEE Transactions on Wireless Communications*, vol. 18, no. 8, pp. 4103–4115, 2019.

[30] S. K. Saha, Y. Ghasempour, M. K. Haider, T. Siddiqui, P. De Melo, N. Somanchi, L. Zakrajsek, A. Singh, O. Torres, D. Uvaydov *et al.*, "X60: A programmable testbed for wideband 60 ghz wlans with phased arrays," in *Proceedings of the 11th Workshop on Wireless Network Testbeds, Experimental evaluation & CHaracterization*. ACM, 2017, pp. 75–82.

[31] P. Sen and J. M. Jornet, "Experimental demonstration of ultra-broadband wireless communi- cations at true terahertz frequencies," in *2019 IEEE 20th International Workshop on Signal Processing Advances in Wireless Communications (SPAWC)*. IEEE, 2019, pp. 1–5.

[32] H. Jiang, P. Wilford *et al.*, "A hierarchical modulation for upgrading digital broadcast systems," *IEEE Transactions on Broadcasting*, vol. 51, no. 2, pp. 223–229, 2005.

[33] Z. Hossain and J. M. Jornet, "Hierarchical bandwidth modulation for ultra-broadband terahertz communications," in *Proc. of the 2019 IEEE International Conference on Communications (ICC)*, Shanghai, P.R. China, May 2019.

[34] U.S. Air Force, "Air force future operating concept: A view of the air force in 2035," Sep. 2015.

[35] N. T. Golmie, "Future generation wireless research and development gaps report," Special Publication (NIST SP) - 1219, Tech. Rep., 2018.

7 LIST OF ACRONYMS

ADC Analog to Digital Converter
AFOSR Air Force Office of Scientific Research AFRL Air Force Research Laboratory
AWG Arbitrary Waveform Generator BiCMOS Bipolar CMOS
BPSK Binary Phase Shift Keying
CMOS Complementary Metal–Oxide–Semiconductor CCF Computing and Communication Foundations CNS Computer and Network Systems
CRI Computer and Information Science and Engineering Research Infrastructure DAC Digital to Analog Converter
DMA Direct Memory Access
DSO Digital Storage Oscilloscope
FPGA Field-Programmable Gate Array
Hb-N Hexagonal Boron Nitride
HBT Heterojunction Bipolar Transistor
HEMT High-Electron-Mobility Transistor IF Intermediate Frequency
LO Local Oscillator
mHEMT Metamorphic High-Electron-Mobility Transistor
MIMO Multiple-Input Multiple-Output
MoS2 Molybdenum disulfide
NASA JPL National Aeronautics and Space Administration Jet Propulsion Laboratory NI National Instruments
NSF National Science Foundation
OFDM Orthogonal Frequency-Division Multiplexing
PSK Phase Shift Keying
PXIe Peripheral Component Interconnect eXtensions for Instrumentation PD Probability of Detection
PI Probability of Intercept
PSG Performance Signal Generator
QAM Quadrature Amplitude Modulation
QCL Quantum Cascade Laser
QPSK Quadrature Phase Shift Keying
RF Radio Frequency
SER Symbol Error Rate
SNR Signal-to-Noise Ratio
TBPS Terabit-per-second
TDMA Time-Division Multiple Access
USAF United States Air Force VDI Virginia Diodes Inc.